Robust Classification of MR Brain Images Based on Multiscale Geometric Analysis

Sudeb Das and Malay Kumar Kundu

Machine Intelligence Unit, Indian Statistical Institute, Kolkata 700108, India
to.sudeb@gmail.com, malay@isical.ac.in

Abstract. The widely used feature representation scheme for magnetic resonance (MR) image classification based on low-frequency subband (LFS) coefficients of wavelet transform (WT) is ineffective in presence of common MR imaging (MRI) artifacts (small rotation, low dynamic range etc.). The directional information present in the high-frequency subbands (HFSs) can be used to improve the performance. Moreover, little attention has been paid to the newly developed multiscale geometric analysis (MGA) tools (curvelet, contourlet, and ripplet etc.) in classifying brain MR images. In this paper, we compare various multiresolution analysis (MRA)/MGA transforms, such as traditional WT, curvelet, contourlet and ripplet, for brain MR image classification. Both the LFS and the high-frequency subbands (HFSs) are used to construct image representative feature vector invariant to common MRI artifacts. The investigations include the effect of different decomposition levels and filters on classification performance. By comparing results, we give the best candidate for classifying brain MR images in presence of common artifacts.

1 Introduction

Recently, magnetic resonance imaging (MRI) has emerged as one of the popular choice to study the human brain [1, 2]. However, because of the huge amount of imaging data, the existing manual methods of analysis and interpretation of brain images are tedious, time consuming, costly and subject to the experience of human observer. This necessitates the requirement of developing automated diagnosis tools to draw quicker and easier inferences from the MR images [3]. Various approaches of brain MR image classification are proposed by different researchers [3–8]. The general framework for classifying brain MR images mainly consists of three phases: (*a*) feature extraction, (*b*) feature reduction and (*c*) classification. The performances of the last two phases greatly depend on the effectiveness of the feature extraction phase. Most of the existing techniques use variants of wavelet transform (WT) for brain MR image's feature extraction. The coefficients of the low frequency subband (LFS) obtained after discrete WT (DWT) decomposition are used as the image representative feature vector. WT works effectively for brain MR images free from common MRI artifacts (small rotation, low dynamic range etc.), but fails in presence of these MRI artifacts.

P. Maji et al. (Eds.): PReMI 2013, LNCS 8251, pp. 482–488, 2013.

WT and related classical MRA transforms suffer from several shortcomings: limited directionality, non-supportiveness to anisotropy etc. To solve these problems, some new multiscale geometric analysis (MGA) transforms such as curvelet (CVT), contourlet (CNT) and type-I ripplet (RT) are introduced [10–12]. These transforms provide superior results than traditional WT in many image processing applications. However, the effectiveness of these MGA transforms for brain MR image classification is not explored still. Our prime objective in this article is to construct an image representative feature vector invariant to these common MRI artifacts, and to compare the performance of different MRA/MGA tools using the same for brain MR image classification.

The rest of this paper is organized as follows. In Section 2, brief reviews of different MRA/MGA transforms are presented. In Section 3, we give the general classification framework for brain MR images and the novel feature extraction scheme. Section 4 presents details of numerical experiments and discussions on the results. Finally, conclusion is drawn in Section 5.

2 Multiresolution Image Decomposition

The MRA/MGA transforms investigated in this article are DWT, CVT, CNT and RT. In this section we briefly review these transforms.

2.1 Discrete Wavelet Transform

The advantage of wavelet is that it performs an MRA of a signal with localization in both time and frequency [9]. In addition to this, functions with discontinuities and functions with sharp spikes require fewer wavelet basis vectors in the wavelet domain than sine cosine basis vectors to achieve a comparable approximation. Discrete wavelet transform (DWT) can be implemented as a set of high-pass and low-pass filter banks. In standard dyadic wavelet decomposition, the output from the low-pass filter can subsequently be decomposed in the same way and the process continues to have finer resolution.

2.2 Curvelet Transform (CVT)

Traditional WT is unable to resolve 2-D singularities along arbitrarily shaped curves, and as a result cannot capture curves and edges of images effectively. To overcome this problem, Candes et al. proposed the CVT with the idea of representing a curve as a superposition of bases of various lengths and widths obeying the scaling law $width \approx length^2$ [10]. CVT uses a parabolic scaling law to achieve anisotropic directionality. A curvelet coefficient can be expressed as the inner product between an element $f \in L^2(R^2)$ and curvelet $\varphi_{j,l,k}$:

$$c(j,l,k) = < f, \varphi_{j,l,k} > = \int_{R^2} f(x)\overline{\varphi_{j,l,k}} dx = \frac{1}{2\pi^2} \int \widehat{f}(w) U_j(R_{\theta_l} w) e^{i < x_k^{(j,l)w} >} dw \quad (1)$$

where, $j = 0, 1, 2, ...$ is a scale parameter; $l = 0, 1, 2, 3, ...$ is an orientation parameter; and $k = (k_1, k_2), k_1, k_2 \ \epsilon \ \mathfrak{T}$ is a translation parameter. The $\varphi_j(x)$ is defined by means of its Fourier transform $\widehat{\varphi_j}(\omega) = U_j(\omega)$, where U_j is frequency window defined in the polar coordinate system $U_j(r,\theta) = 2^{\frac{-3j}{4}} W(2^{-j}r)V(\frac{2\lfloor \frac{j}{2} \rfloor \theta}{2\pi})$ where, W and V are the radial and angular windows obeying the admissibility conditions, respectively. Curvelets at scale 2^{-j}, orientation θ_l and position $x_k^{(j,l)} = R_{\theta_l}^{-1}(k_1 \cdot 2^j, k_2 \cdot 2^{\frac{-j}{2}})$ can be expressed as: $\varphi_{j,l,k}(x) = \varphi(R_{\theta_l}(x - x_k^{(j,l)}))$, where $\theta_l = 2\pi \cdot 2^{\lfloor \frac{j}{2} \rfloor} \cdot l$, with $l = 0, 1, ..., 0 \leq \theta_l < 2\pi$,$R_{\theta_l}$ is the rotation by θ_l radians. The actual implementation of the CVT is as follows: (i) apply the 2D FFT and obtain Fourier samples, (ii) form the product by multiplying the discrete localizing window $U_{j,l}$ for each scale j and angle l, (iii) wrap this product around the origin, (iv) apply the inverse 2D FFT to collect the discrete coefficients $c^D(j,l,k)$.

2.3 Contourlet Transform (CNT)

CNT gives a multiresolution, local and directional expansion of image using Pyramidal Directional Filter Bank (PDFB) [11]. The PDFB combines Laplacian pyramid (LP) which captures the point discontinuities, with a directional filter bank (DFB) which links these discontinuities into linear structures. LP is a multiscale decomposition of $L^2(R^2)$ into series of increasing resolution subspaces which are orthogonal complements of each other as follows: $L^2(R^2) = V_{j_0} \oplus (\bigoplus_{j=J_0}^{-\infty} W_j)$. An l-level DFB generates a local directional basis for $l^2(Z^2)$ that is composed of the impulse responses of the DFBs and their shifts. In CNT, the directional filter is applied to the detail subspace W_j. This results in a decomposition of W_j into 2^{l_j} subspaces at scale 2^j: $W_j = \bigoplus_{k=0}^{2^{l_j - 1}} W_{j,k}^{l_j}$.

2.4 Ripplet Transform Type - I(RT)

To generalize the scaling law of the CVT and to find out which scaling law will be optimal for all types of boundaries Xu et al. proposed the RT. RT generalizes CVT by adding two parameters: support c and degree d [12]. CVT is a special case of RT with $c = 1$ and $d = 2$. In the frequency domain, the frequency response of ripplet function is in the form: $\widehat{\rho_j}(r,\omega) = \frac{1}{\sqrt{c}} a^{\frac{m+n}{2n}} W(2^{-j} \cdot r)V(\frac{1}{c} \cdot 2^{-\lfloor j \frac{m-n}{n} \rfloor} \cdot \omega - l)$ where, W and V are the 'radial' and 'angular' windows, respectively satisfying the admissibility conditions. a_j, $\overrightarrow{b}_k$ and θ_l represents the scale, position and rotation parameters, respectively and satisfy that $a_j = 2^{-j}$, $\overrightarrow{b}_k = [c \cdot 2^{-j} \cdot k_1, 2^{-j/d} \cdot k_2]^T$ and $\theta_l = \frac{2\Pi}{c} \cdot 2^{-\lfloor j(1-1/d) \rfloor} \cdot l$, where $\overrightarrow{k} = [k_1, k_2]^T$, and j, k_1, k_2, $l \in \mathbb{Z}$. $(\cdot)^T$ denotes the transpose of a vector. The 'wedge' corresponding to the ripplet function in the frequency domain is: $H_{j,l}(r,\theta) = \{2^j \leq |r| \leq 2^{2j}, |\theta - \frac{\pi}{c} \cdot 2^{-\lfloor j(1-1/d) \rfloor} \cdot l| \leq \frac{\pi}{2} 2^{-j}\}$. The DRT of an $M \times N$ image $f(n_1, n_2)$ is in the form of

$$R_{j,\overrightarrow{k},l} = \sum_{n_1=0}^{M-1} \sum_{n_2=0}^{N-1} f(n_1,n_2) \overline{\rho_{j,\overrightarrow{k},l}(n_1,n_2)} \tag{2}$$

where $R_{j,\overrightarrow{k},l}$ are the ripplet coefficients and $\overline{(.)}$ denotes the conjugate operator.

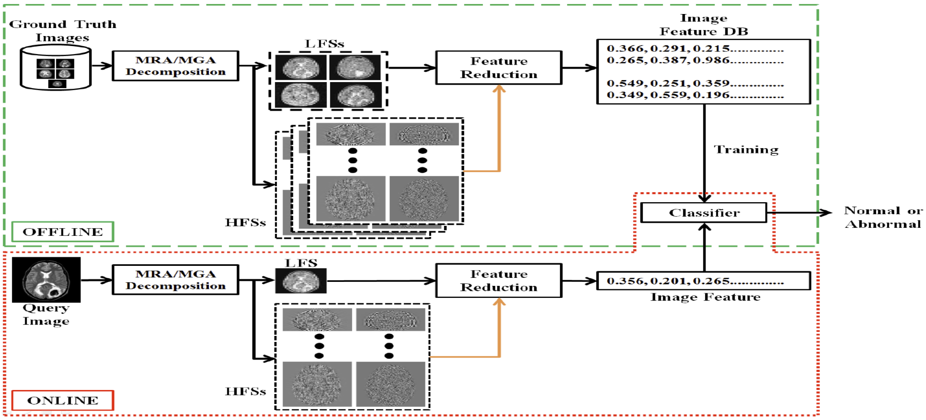

Fig. 1. Block diagram of the general framework for brain MRI classification

3 General Framework for Brain MRI Classification

The block diagram of the Fig. 1 shows the general framework for brain MRI classification. Different MRA/MGA transforms are used in the first phase for feature extraction. The high dimensionality of the feature vector is reduced by principal component analysis (PCA) during the second phase. In the third phase, various classification techniques are used to classify the brain MR image into normal and abnormal classes [3–8].

Small rotation, low dynamic range, noise etc. are the common artifacts present in today's MR images. The existing brain MR image classification schemes work efficiently for images free from common MRI artifacts, but their performance decrease in presence of these artifacts. The commonly used LFS for representing MR images is ineffective in capturing the subtle details and directional information present in the images. To tackle this problem, in this article we propose to use both the LFS and HFSs coefficients during feature extraction. After decomposing the images of the training set through a MRA/MGA transform, the subband's energy for each HFSs are calculated as follows:

$$ENG_s^d = \frac{1}{M \times L} \sum_{x=1}^{M} \sum_{y=1}^{L} |I_s^d(x,y)|^2 \tag{3}$$

where, I_s^d is the subband of size $M \times L$ at scale s and direction d, $s = 1, 2, ..., S$, $d = 1, 2, ..., D$. Then the coefficients of the LFSs and the HFSs energies' are passed to PCA for feature reduction, which results in the feature vector of dimension 10 (this value is chosen experimentally). The novel use of HFSs information for feature representation is indicated by "orange" colored lines in the block diagram of Fig. 1.

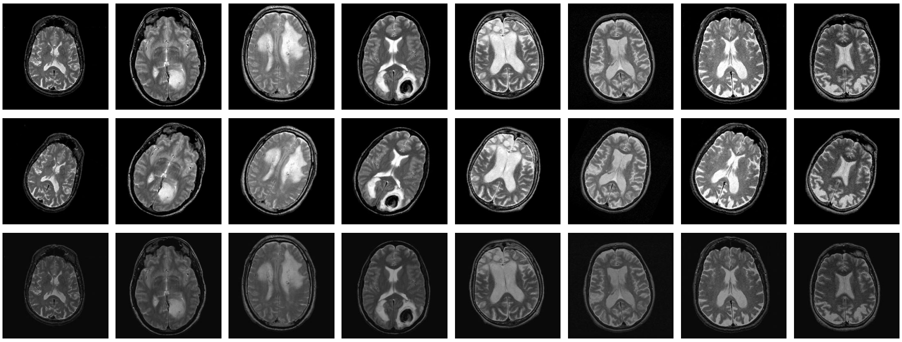

(a) (b) (c) (d) (e) (f) (g) (h)

Fig. 2. Sample brain MR images (row 1) with corresponding rotated (row 2) and dynamic range (row 3) modified versions: (a) normal, (b) glioma, (c) meningioma, (d) sarcoma, (e) Pick's disease, (f) Huntington's disease, (g) Alzheimer's disease, (h) Alzheimer's disease with visual agnosia

4 Experimental Results and Comparisons

The dataset used in the experiments consists of 66 T2-weighted MR brain images in axial plane, free from common MRI artifacts (downloaded from the website of Harvard Medical School URL:http://med.harvard.edu/AANLIB/). This dataset consists of 18 normal and 48 abnormal brain MR images. The abnormal brain MR images of the datasets includes images of the following diseases: glioma, meningioma, Alzheimer's disease, Alzheimer's disease plus visual agnosia, Pick's disease, sarcoma and Huntington's disease. The training set images are rotated through 5 different angles $5°$ to $25°$ in clockwise direction, and the dynamic ranges of the images are modified to 5 different levels (150,10) to (250,30), respectively. Therefore, the total number of images in the dataset used in the experiments is 726. To compare the performance of the DWT using different numbers of decomposition levels and wavelet bases, we consider 3 wavelet families: Daubechies (dbN, N = 1, 8), Coiflets (coifN, N = 1, 5), and Biorthogonal (biorN.N, N.N = 1.3, 6.8). For each wavelet basis, the number of decomposition levels from 1 to 4 is considered. For the other three transforms, 6 different pyramidal and directional filter combinations (from {'9/7', '5/3'} and {'9/7', '5/3', 'pkva'}) are considered with different number of decomposition levels. To classify the images k-nearest neighbor (k-NN) classifier is used with $k = 1$. To avoid overfitting problem, we integrate K-fold cross validation into our method ($K = 5$), which make the proposed scheme reliable and generalize to other independent datasets. Fig. 2, shows samples of the brain MR images used in the experiments.

We consider different number of principal components (PCs) to reduce the dimension of the feature vector. After extensive experiments we have found that 10 number of PCs (preserving $> 80\%$ of the total variance) is providing acceptable results. Therefore, in this article we compare the different MRA/MGA transforms considering only 10 PCs.

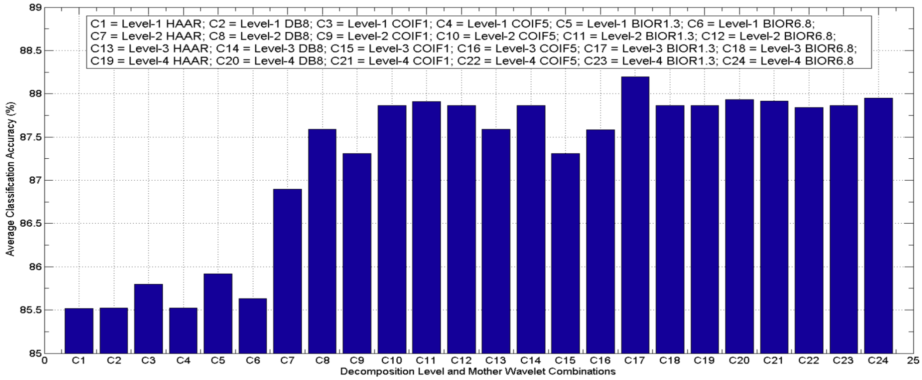

Fig. 3. Performance comparison of different wavelet combinations

Fig. 3 illustrates the performance comparison of WT with different decomposition levels and mother wavelets. For CNT, CVT and RT the best results are obtained for decomposition orientations $\{4, 8, 8\}$, $\{4, 4\}$ and $\{2, 4\}$, respectively. The graph of Fig. 4 shows the results for CNT, CVT and RT with different filter combinations and the above mentioned best decomposition orientations. The

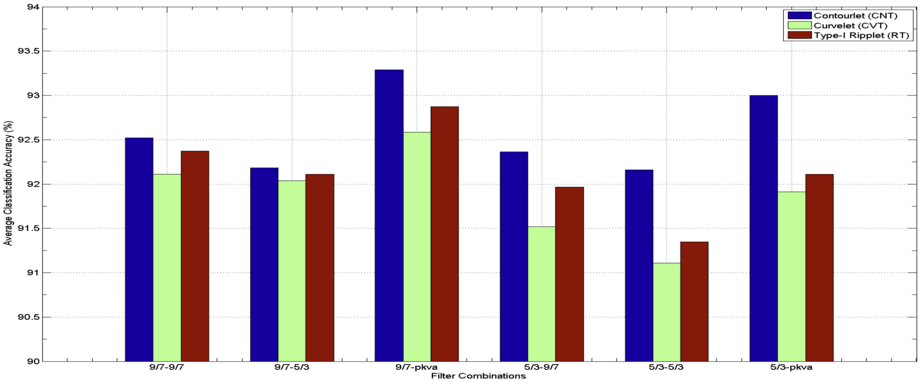

Fig. 4. Performance comparison of CNT, CVT and RT

graph of Fig. 3, shows that 'bior1.3' mother wavelet at decomposition level 3 provides the best performance ($\approx 88\%$) among different WT configurations. This is because of the high smoothness, small support, high vanishing moments, linear phase and near orthogonal properties of 'bior' wavelet compared to others. The performance decreases near about $10\% - 12\%$, when we only used LFS features for classification. From the graph of Fig. 4, it can be clearly seen that the filter combination '9/7' (pyramidal) and 'pkva' (directional) performs the best for CNT, CVT and RT. The '9/7' filters are linear phase and are close to being orthogonal and thus carries more subtle image information. Whereas, the ladder structure 'pkva' filters are more effective because of its superior edge direction localization property. Moreover, among these three transforms CNT performs the best in terms of average classification accuracy of $\geq 93\%$. When we used only LFS features obtained from these three transforms for classification, the performance decreases near about $6\% - 7\%$.

5 Conclusions

Existing techniques for classifying brain MR images perform poorly in presence of common MRI artifacts. The directional information present in HFSs along with the LFS features prove effective in these scenarios. Moreover, recent advanced transforms perform much better than the conventional WT in classifying brain MR images. Comparative study of the performances of these transforms show that CNT performs superiorly considering both the classification accuracy and the dimension of the feature vector.

References

1. Westbrook, C.: Handbook of MRI Technique. John Wiley & Sons (2008)
2. Rombouts, S. A., Barkhof, F., Scheltens, P.: Clinical Applications of Functional Brain MRI. Oxford University Press (2007)
3. Zhang, Y., Wu, L.: An MR brain images classifier via principal component analysis and kernel support vector machine. Progress In Electromagnetics Research 130, 369–388 (2012)
4. Chaplot, S., Patnaik, L.M., Jagannathan, N.R.: Classification magnetic resonance brain images using wavelets as input to support vector machine and neural network. Biomedical Signal Processing and Control 1(1), 86–92 (2006)
5. Maitra, M., Chatterjee, A.: A Slantlet transform based intelligent system for magnetic resonance brain image classification. Biomedical Signal Processing and Control 1(4), 299–306 (2006)
6. Das, S., Chowdhury, M., Kundu, M.K.: Brain MR image classification using multiscale geometric analysis of ripplet. Progress In Electromagnetics Research 137, 1–17 (2013)
7. El-Dahshan, E.-S.A., Hosny, T., Salem, A.-B.M.: Hybrid intelligent techniques for MRI brain images classification. Digital Signal Processing 20(2), 433–441 (2010)
8. Zhang, Y., Dong, Z., Wu, L., Wang, S.: A hybrid method for MRI brain image classification. Expert Systems with Applications 38(8), 10049–10053 (2011)
9. Mallat, S.: A wavelet tour of signal processing: the sparse way, 3rd edn. Academic Press (2008)
10. Candès, E.J., Donoho, D.L.: Curvelets: a surprisingly effective nonadaptive representation for objects with edges. In: Cohen, A., Rabut, C., Schumaker, L.L. (eds.) Curve and Surface Fitting, pp. 105–120. Vanderbilt University Press (2000)
11. Do, M.N., Vetterli, M.: The contourlet transform: an efficient directional multiresolution image representation. IEEE Transaction Image Processing 14(12), 2091–2106 (2005)
12. Xu, J., Yang, L., Wu, D.: Ripplet: A new transform for image processing. Journal of Visual Communication and Image Representation 21(7), 627–639 (2010)